



## Article

# Selective Sulfation Roasting for Cobalt and Lithium Extraction from Industrial LCO-Rich Spent Black Mass

Jayasree Biswas <sup>1,\*</sup> , Sofia Ulmala <sup>1</sup>, Xingbang Wan <sup>2</sup>, Jere Partinen <sup>1</sup>, Mari Lundström <sup>1</sup> and Ari Jokilaakso <sup>1</sup> <sup>1</sup> Department of Chemical and Metallurgical Engineering, School of Chemical Engineering, Aalto University, 02150 Espoo, Finland<sup>2</sup> School of Energy Science and Engineering, Central South University, Changsha 410017, China

\* Correspondence: jayasree.biswas@aalto.fi

**Abstract:** The extraction of cobalt from secondary resources has become crucial, as cobalt has been identified as a strategically important and critical raw material due to the high risks of supply chain disruptions. In this work, selective sulfation roasting was investigated as a potential recycling strategy to extract cobalt and lithium from an industrial lithium cobalt oxide (LCO)-rich black mass. Additionally, the effect of graphite on metal extraction was studied. In the first set of experiments, the sieved black mass fraction containing both cathode and anode materials was directly roasted in a predetermined composition of gas mixtures of SO<sub>2</sub>, O<sub>2</sub>, and Ar for 1 h at 850 °C. The gas composition was determined from Kellogg's diagram to allow for the selective sulfation of Co and Li. In another set of experiments, the carbon present in the black mass was first removed by roasting the material in Ar for 2 h and then in an Ar and O<sub>2</sub> gas mixture for five hours at 600 °C. Afterward, selective sulfation roasting was performed in mixtures of SO<sub>2</sub>, O<sub>2</sub>, and Ar gas similar to the previous set of experiments. For comparison, similar experiments were performed at 800 °C. The sulfation roasted black mass was leached in water to study the efficiency of Co extraction into the solution. Interestingly, the presence of carbon was found to be beneficial for Co extraction. The extraction efficiency for the first case (with carbon present in the raw material) was observed to be more than three times higher than in the second case (with carbon removed) for sulfation at 850 °C. The extraction efficiency and purity of the extracted Co were found to be better for higher temperature sulfation roasting conditions due to faster reaction kinetics. It was also found that almost all of the Li could be recovered while extracting Co. The maximum efficiency of the extraction was 99.51% Li and 61.21% Co for roasting under a gas flow of 10% SO<sub>2</sub>-10% O<sub>2</sub>-Ar at 850 °C for 60 min. These results suggest that Co and Li can be selectively extracted from the black mass by sulfation roasting pre-treatment followed by leaching in water. In holistic processing, the leach residue can then be further subjected to battery metal processing by state-of-the-art methods.

**Keywords:** recycling; lithium-ion battery; cobalt recovery; sulfation roasting; water leaching

**Citation:** Biswas, J.; Ulmala, S.; Wan, X.; Partinen, J.; Lundström, M.; Jokilaakso, A. Selective Sulfation Roasting for Cobalt and Lithium Extraction from Industrial LCO-Rich Spent Black Mass. *Metals* **2023**, *13*, 358. <https://doi.org/10.3390/met13020358>

Academic Editor: Bernd Friedrich

Received: 13 January 2023

Revised: 2 February 2023

Accepted: 7 February 2023

Published: 10 February 2023



**Copyright:** © 2023 by the authors. Licensee MDPI, Basel, Switzerland. This article is an open access article distributed under the terms and conditions of the Creative Commons Attribution (CC BY) license (<https://creativecommons.org/licenses/by/4.0/>).

## 1. Introduction

The worldwide transition towards a green economy is boosting the market for lithium-ion batteries (LIBs), and the global demand for LIBs is predicted to increase to 9300 GWh by 2030 [1]. The widespread application of LIBs is growing, from electronics to electric vehicles, due to their superior electrochemical properties, such as high energy density and low self-discharge rates. This skyrocketing demand for LIBs has the potential to disrupt the supply chain of raw materials, and the criticality of this situation has already been identified by several countries.

The estimated lifespan of LIBs is typically 2–3 years for consumer electronics and >10 years for electric vehicles [2,3]. With the growing consumption of portable electronics and electric vehicles, a huge volume of mixed-type battery waste will be generated. By the end of 2020, 17.6 GWh of batteries had already attained their end of life, and this is expected

to rise to 140 GWh by 2035 [4]. Spent LIBs contain valuable metals ranging between 5% and 20% Co, 5% and 10% Ni, 5% and 7% Li, and 6% and 12% Cu [5]. Although the popularity of lithium nickel manganese cobalt oxide (NMC), lithium iron phosphate (LFP), or lithium nickel cobalt aluminum oxide (NCA) batteries is predicted to rise in the future, the LCO battery sales accounted for the largest revenue share of over 30% in 2021 [6], which will generate large volumes of spent LCO battery scrap within a few years. Therefore, the recycling of these spent LIBs (specifically spent LCO-based batteries) is necessary and can be an additional source of Co, which is one of the most expensive metals. Despite this, currently, only less than 5% of these spent LIB batteries are recycled [7] globally, with the remainder going to landfills. The toxic chemicals and heavy metals from these batteries could contaminate the soil and underground water, threatening the ecosystem and human health. The key reasons for this low recycling rate are deficient legislation, poor collection systems, and the lack of viable recycling technology for the rapidly changing compositions of battery scrap.

In recent times, global attention has been drawn to the necessity of recycling LIBs scrap and developing feasible technologies. Furthermore, battery recycling is also encouraged by governments by introducing legislation through directives and defining targets for collection and recycling rates. This was pioneered by China, which imposed legislation to control solid waste pollution in 1995, followed by the USA, EU, Japan, and other countries. In the battery directive 2006/66/EC [8], the EU defined a 70% recycling rate target for spent LIB batteries and a recovery rate of 70% for Li and 90% for Co, Ni, and Cu by 2030. The major components of LIBs are separators, casings, electrolytes, current collectors, and electrodes. Generally, pretreatments such as discharging, dismantling, and mechanical processing, e.g., sorting, crushing, milling, and sieving, are performed to produce battery fractions for further refining. The fraction known as “black mass”—which is rich in active materials—is predominantly refined via metallurgical routes, consisting either of pyrometallurgical unit processes (smelting, roasting) followed by hydrometallurgical refining or black mass, which can be directly subjected to hydrometallurgical refining. Typical hydrometallurgical processes in battery recycling consist of acid leaching, the chemical deposition of impurities, solvent extraction for valuable metals separation, and, finally, crystallization for battery-grade salt recovery. Alternatively, metals can be recovered in metallic form using electrolysis. Several research studies [9–16] have been conducted to extract Li and Co from LIB scrap using acid leaching and solvent extraction techniques. The influence of additional pretreatments, such as carbothermic reduction [17] or thermal pretreatment [18,19], before leaching has also been investigated to improve the efficiency of metal recovery in hydrometallurgical processing. Despite the fact that the efficiency of metals recovery from spent battery scrap is very high for hydrometallurgical routes, the main drawback is the consumption of a high volume of concentrated acids and water [20].

Pyrometallurgical processes include medium-temperature processes, such as roasting, and high-temperature processes, such as smelting. Depending upon the atmospheric conditions, different types of roasting can be applied, including reduction roasting, chlorination roasting, nitration roasting, and sulfation roasting. Reduction roasting and sulfation roasting have been studied the most in terms of LIB scrap recycling. In the reduction roasting process, the active cathode material of spent LIBs is heated, typically in a temperature range of 500 °C to 1000 °C, with a reducing agent such as charcoal, coke, lignite, or graphite under a controlled atmosphere. This results in a mixture of  $\text{Li}_2\text{CO}_3$  and metallic Co [21–25] or a Co/CoO [26] mixture, or some other metal or metal oxides [27] such as Ni, MnO, etc., depending on the amount of the reducing agent. Some researchers introduced additional conditions, such as Tang et al. [26], who performed vacuum pyrolysis before reduction roasting, and Peng et al. [28], who purged steam to facilitate a reduction in roasting efficiency. This process has high extraction efficiency, although the presence of carbon in the roasted product introduces problems in the leaching process. Instead of using carbon as a reducing agent, Wang et al. [29,30] studied the in situ thermite reduction in spent LIB cathodes by aluminum foil in combination with leaching and achieved a Li, Co,

and Al recovery efficiency of more than 90%. In the smelting reduction process, spent LIB scrap is heated above its melting point in a furnace in the presence of reducing and fluxing agents to separate it into a Fe-Ni-Co-Cu-based alloy and slag containing Li and the remaining elements [31–33]. Apart from lab-scale research, this smelting reduction technology, in combination with additional pretreatment and hydrometallurgical treatment is widely accepted by the industry, e.g., Umicore Vales [34], Sumitomo-Sony, and Accurec GmbH [35]. Although this smelting reduction is advantageous in the sense that there is not much preprocessing required, it is a highly energy-intensive process [36,37]. To overcome this, nowadays, attention is being paid to medium-temperature roasting processes. Chlorination roasting with water leaching has been studied by several researchers [38–42] using the addition of  $\text{NH}_4\text{Cl}$  salt or  $\text{Cl}_2$  gas at a medium temperature (300 °C to 900 °C) and achieving a Li, Co, Ni, and Mn extraction efficiency of almost 100% [39]. Sulfation roasting followed by water leaching is well-established for processing sulfide ores. Typically, studied sulfating agents for spent LIB scrap processing are sulfur-containing gas such as  $\text{SO}_2$  [43], sulfate salts such as  $\text{MgSO}_4$ ,  $(\text{NH}_4)_2\text{SO}_4$  [44,45],  $\text{NaHSO}_4 \cdot \text{H}_2\text{O}$  [46], or  $\text{Na}_2\text{SO}_4$  and sulfuric acid [47–49]. The extraction efficiency obtained has been as high as 99% Li and 98% Co. The present authors have selected this sulfation roasting by  $\text{SO}_2$ -based gas followed by a water-leaching route to extract valuable metals from spent LIBs. The main advantage of this proposed process is that sulfates are easily soluble in water, and toxic acid consumption can be avoided. In the conventional smelting-based pyrometallurgical processes, Li is lost mainly in the slag. Using this route, by carefully controlling the atmosphere, there is the possibility of the selective formation of metal sulfates, thus enabling selective extraction. The main challenge is in the thermodynamic closeness of various sulfates, which makes single-element sulfation difficult, requiring controlled operating conditions and accurate knowledge of the reaction mechanism and kinetics. Therefore, a novel integrated approach and a sequential selective sulfation roasting unit process is the final target of this investigation. In a previous work [43] in the authors' laboratory, sulfation roasting was studied with synthetic  $\text{LiCoO}_2$  powder, and a very low recovery (only 17.4%) of Co was obtained. However, the scenario could be different with real battery scrap, and this was the motivation for the current research.

In this work, an investigation was performed on the sulfation roasting of spent Co-rich LIB scrap with an  $\text{SO}_2$ - $\text{O}_2$ -Ar gas mixture to extract Co and Li selectively. Black mass from spent LIB scrap was roasted under a flow of a mixture of  $\text{SO}_2$ - $\text{O}_2$ -Ar gases, followed by leaching in water to study the efficiency of Co and Li extraction. The influence of graphite on the kinetics of sulfation roasting was also investigated.

## 2. Experimental Technique

### 2.1. Materials

This study was conducted with original battery scrap which was supplied by AkkuSer Oy (Nivala, Finland). In the industrial process [50], the waste battery scrap was sorted, crushed, and sieved into size fractions (<1000  $\mu\text{m}$ ). The company supplied underflow fractions, which were further processed in a vibratory sieve shaker (Fritsch, Analysette 3, Idar-Oberstein, Germany) in the authors' laboratory. Samples of a mass fraction of <125  $\mu\text{m}$  were used for the sulfation roasting experiments. It was shown in a previous study [51] that this size fraction contains much less Cu and Al, which substantially increase in larger size fractions. This size fraction was almost 41% of the total mass of the battery scrap and was comparatively more homogeneous than the other size fractions. Additionally, on the larger-sized particles, there is the possibility of the formation of a product layer of sulfates, which could slow down the sulfation kinetics. Therefore, in this work, the mass transfer through the product layer in the stationary bed of solid material was minimized by selecting the <125  $\mu\text{m}$  size fraction, which consisted of mainly cathode and anode fractions, i.e., black mass. High-purity  $\text{O}_2$  (99.99%),  $\text{SO}_2$  (99.99%), and Ar (99.999%) gases were used for the sulfation roasting experiments.

## 2.2. Roasting Apparatus

The experimental setup shown in Figure 1 consists of a horizontal tube furnace (Lenton, Parsons Lane, Hope, UK) which was equipped with a silicon carbide heating element and an alumina tube with an inner diameter of 44 mm. The furnace was connected to a gas inlet, which was coupled with DFC digital mass flow controllers (Aalborg, Orangeburg, New York, NY, USA) to mix  $O_2$  (99.99%),  $SO_2$  (99.99%), and Ar (99.999%) gases to achieve the desired atmosphere in the furnace. An S-type thermocouple (Johnson-Matthey Noble Metals, Royston, UK) was placed in the hot zone of the furnace to measure the temperature, and a Keithley 2000 multimeter (Keithley, Solon, OH, USA) intelligent temperature controller was installed to monitor the temperature continuously. The gas outlet from the furnace was passed through a NaOH solution to absorb the remaining  $SO_2$  gases before being released into the fume hood. Both ends of the furnace tube were connected to water cooling channels.

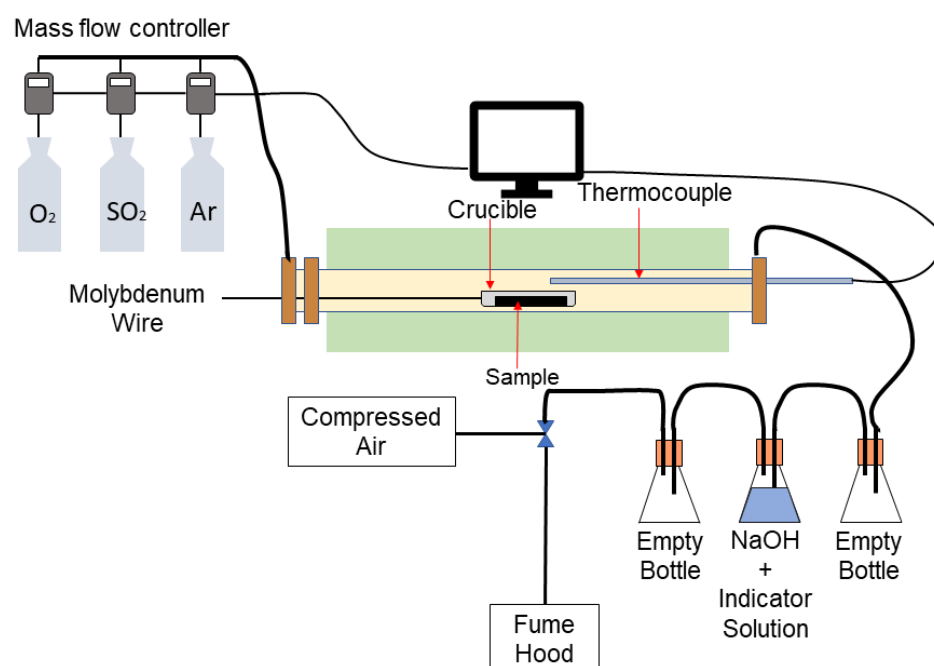


**Figure 1.** Schematic of sulfation roasting experimental setup.

## 2.3. Procedure

The furnace was heated to the target temperature, and a silica boat containing 4 g of spent black mass was placed in the cold zone of the furnace. Then, the furnace was sealed, and an argon gas flow of 500 mL/min was maintained for the initial 10 min to remove the remaining air in the furnace. Thereafter, the silica boat was pushed slowly into the hot zone of the furnace. In this research work, two types of experiments were performed.

In the first type of experiment, the samples were directly roasted under a 500 mL/min gas flow comprising  $O_2$ ,  $SO_2$ , and Ar for the target time period at two different temperatures (800 °C and 850 °C). The gas composition was determined from the thermodynamic stability diagram, which is discussed in later sections. After the completion of sulfation roasting, the silica boat was pulled rapidly into the cold zone of the furnace. Thereafter, the gas flow was switched from the  $O_2$ ,  $SO_2$ , and Ar gas mixture to a 100% Ar gas flow. A few minutes later, the sample was taken out of the furnace.

In the second type of experiment, pre-roasting was performed in two stages: first, for two hours at 600 °C under a 500 mL/min argon flow, and second, five hours of roasting under a 500 mL/min argon (80%) and oxygen (20%) gas mixture at the same temperature. This additional pre-roasting was performed to burn the graphite present in the spent black mass. After pre-roasting was complete, a similar procedure was followed

for the sulfation roasting of the pre-roasted spent black mass at two different temperatures (800 °C and 850 °C).

The sulfation roasted samples were further characterized by X-ray diffraction (X'Pert Pro MPD, PANalytical, Almelo, The Netherlands) and scanning electron microscopy (SEM, Mira3, Tescan, Brno, Czech Republic), and water leaching was performed at 60 °C for 90 min with a solid-to-liquid ratio of 100 g/L. In this water-leaching process, 2 g of sulfation roasted samples from each experiment were dissolved into 20 mL of water in an Erlenmeyer flask (25 mL) in the above-mentioned conditions, and the solution was continuously stirred with a magnetic stirrer (300 RPM) for 90 min. Thereafter, the leach residue was filtered, and the solution was analyzed by atomic absorption spectroscopy (AAS, Thermo Scientific iCE 3000, Waltham, MA, USA). To calculate the extraction efficiency, the leach residue was further digested with a concentrated aqua regia solution in which hydrochloric acid (37%, Merck Sigma-Aldrich, Helsinki, Finland) and nitric acid (65%, Merck Supelco, Espoo, Finland) were combined in a molar ratio of HCl: HNO<sub>3</sub> = 3:1. If the residue mass was greater than 0.5 g, 0.5 g of the residue was dissolved into 50 mL of the solution. Otherwise, all of the residue mass was dissolved into 50 mL of solution. Thereafter, the residue-digested solution was analyzed by atomic absorption spectroscopy (AAS). The overall procedure is presented in a flowchart in Figure 2.

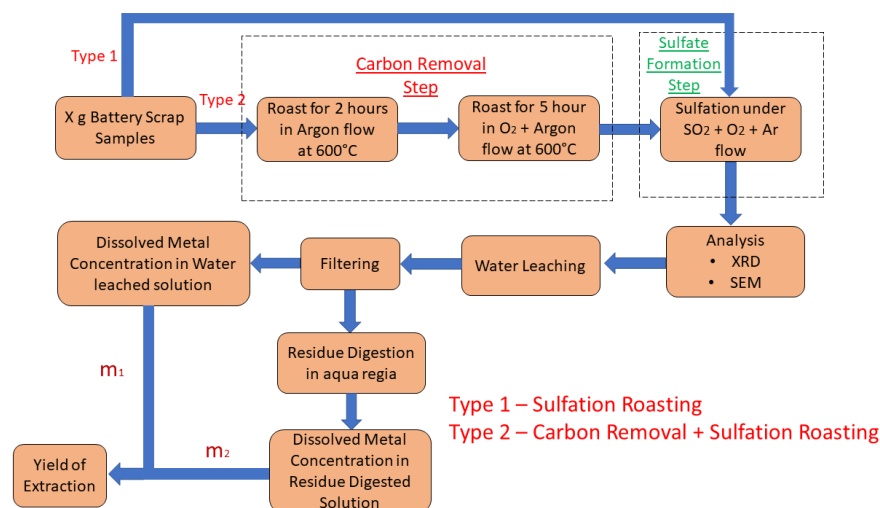


**Figure 2.** Flowchart of the overall experimental procedure.

#### 2.4. Analytical Methods

The metal concentration in the black mass was measured using an inductively coupled plasma optical emission spectroscopy instrument (ICP-OES, iCAP Pro, Thermo Fisher Scientific, Waltham, MA, USA), and the carbon concentration was measured using a LECO combustion analyzer (CS744, LECO Nordic, Sweden). The sulfation roasted black mass was characterized by X-ray diffraction (XRD) with a scan rate of 2°/min from 10° to 90° angles using Cu-K<sub>α</sub> radiation. The XRD data was processed using HighScore Plus software (version 4.8, PANalytical) to identify the phases. The sulfation roasted powdered samples were also characterized using scanning electron microscopy equipped with an energy dispersive spectrometer (UltraDry Silicon Drift EDS, Thermo Fisher Scientific, Waltham, MA, USA) to determine the composition of Co, Ni, Cu, Mn, O, and S. An accelerating voltage of 15 kV and a beam current of 10 nA were applied on the sample surface for SEM analysis. The following standards: Co (K<sub>α</sub>, cobalt), Ni (K<sub>α</sub>, nickel), Cu (K<sub>α</sub>, copper), Mn (K<sub>α</sub>, manganese), O (K<sub>α</sub>, diopside), and S (K<sub>α</sub>, marcasite), were used in NSS microanalysis software for composition analysis. The water-leached sample solution and the residue-digested solution were analyzed using atomic absorption spectroscopy (AAS) to determine the concentration of Co, Li, Ni, Mn, Cu, and Fe. The yield of extraction was calculated from



the metal concentration obtained from AAS for the water-leached solution and residue-digested solution. The yield of extraction could be calculated as:

$$\% \text{ extraction} = \frac{m_1}{m_1 + m_2} \times 100\% \quad (1)$$

where  $m_1$  is the mass of the specific metal which formed sulfates and dissolved into water, and  $m_2$  is the mass of the specific metal remaining in the residue.

### 3. Results and Discussion

#### 3.1. Characterization of LIB Waste

The XRD pattern presented in Figure 3 shows that the black mass studied here consists of three main phases— $\text{LiCoO}_2$ ,  $\text{Li}(\text{Mn}_{0.33}\text{Co}_{0.33}\text{Ni}_{0.33})\text{O}_2$ , and graphite (as carbon). Cobalt originates from the battery cathode, and graphite from the anode. The composition analysis of the black mass, presented in Table 1, shows a high concentration of Co (~27%), which is due to the presence of mostly  $\text{LiCoO}_2$  and a very small quantity of  $\text{Li}(\text{Mn}_{0.33}\text{Co}_{0.33}\text{Ni}_{0.33})\text{O}_2$ . The composition analysis also suggests the presence of other metals, such as Cu, Fe, and Al, which could originate from the casing or current collectors. Co is the most expensive metal among all the elements present in the black mass (one metric ton of black mass equivalent to Co is valued at 20,000 USD according to the May 2022 price). Table 1 also shows the presence of a high concentration of carbon (33%) in the black mass. A particle size distribution analysis for the LCO-rich battery scrap (<125  $\mu\text{m}$ ) was performed using a laser diffraction particle size analyzer (Mastersizer 3000, Malvern, UK) and is presented in Figure 4a,b. The particle size distribution in Figure 4a shows a bimodal distribution. As shown in Figure 4a,b, 70% of the volume of the scrap fraction is <125  $\mu\text{m}$  in size and has a mean size of ~30  $\mu\text{m}$ . However, the powdered battery scrap also contains small foil-like particles of Cu and Al, which mainly originate from the current collector foils of the batteries. Since one of the dimensions of these foil-shaped particles is less than 125  $\mu\text{m}$ , it can easily pass through the 125  $\mu\text{m}$  sieve during the sieve analysis. Therefore, another peak can be observed in Figure 4a. Previously in the authors' laboratory [52], a detailed analysis of LCO-rich scrap was conducted, in which five samples were considered for chemical composition analysis. It was observed that the standard deviation of the particles was large for Cu and Al. The current investigation also suggests a similar observation. By selecting a smaller particle size fraction (<125  $\mu\text{m}$ ) for analysis, the extent of heterogeneity was minimized.

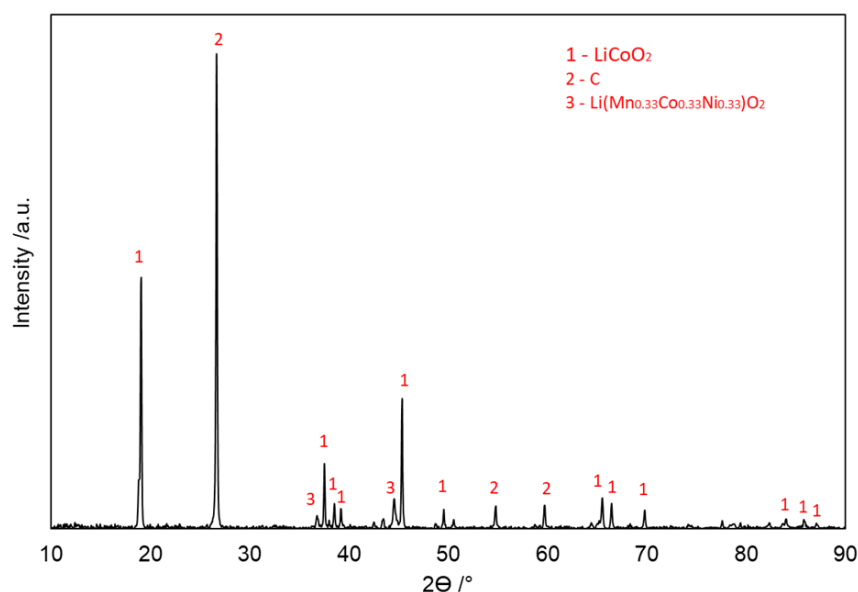
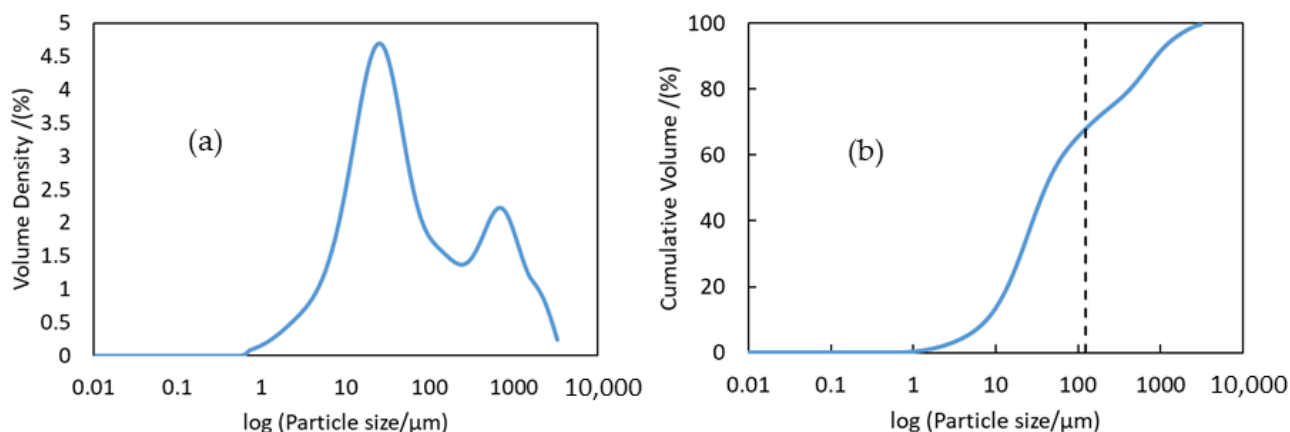


Figure 3. XRD analysis of LCO-rich spent black mass provided by industry.

**Table 1.** Composition analysis (wt.%) of the original battery scrap. The term “rest” denotes the residual materials.

Elements	Al	Ca	Co	Cu	Fe	K	Li	Mg	Mn	Na	Ni	P	Zn	C	Rest
wt.%	1.64	0.03	26.45	2.72	0.61	0.05	3.87	0.09	1.67	0.06	2.74	0.45	0.04	33	26.58

**Figure 4.** Particle size distribution plotted in (a) Volume density percentage against particle size on the logarithmic scale in blue line and (b) Cumulative distribution against particle size on the logarithmic scale in blue line and the black dotted line indicates 125  $\mu\text{m}$  particle size.

### 3.2. Thermodynamics

To determine the selective sulfation conditions, thermodynamic stability conditions were analyzed for the Co-Li-Ni-Cu-Mn-S-O system. It should be noted that the top five metals based on the composition of the black mass presented in Table 1 were selected for thermodynamic analysis. The predominance area diagram, also known as the Kellogg diagram, was obtained for the Co-Li-Ni-Cu-Mn-S-O system using FactSage software (version 8.2) and selecting the FactPS database. Figure 5a presents the predominance diagram of the multi-component system for 850 °C. The equilibrium lines for metal oxides/metal sulfates are plotted with the variation in  $\text{O}_2$  and  $\text{SO}_2$  partial pressures and were indicated by different colors for different metals. It can be observed that lithium is stable as sulfate ( $\text{Li}_2\text{SO}_4$ ) within this entire range of selected  $\text{SO}_2$ - $\text{O}_2$  conditions. Therefore, the formation of lithium sulfate is unavoidable when cobalt sulfate is formed. According to the stability of the oxide and sulfate phases shown in Figure 5a, the region surrounded by the red and green lines could be selected for the formation of sulfates of Co and Li, whereas the other metals would remain oxides. Similarly, this analysis was performed for 800 °C, and the predominance diagram is presented in Figure 5b. From this stability diagram, two experimental conditions were chosen for the selective sulfation of Co and Li, which are marked as A and B in Figure 5a,b for 850 °C and 800 °C, respectively.

The variation in the stability of oxide and sulfate phases with a variation in temperature and  $\text{SO}_2$  partial pressures at a fixed oxygen partial pressure of 0.1 atm is presented in Figure 5c, and the selected experimental conditions are marked. It can be observed that, at lower temperatures, the selectivity of sulfation was lost, and all the metals formed a sulfate. This selective sulfation property is desirable for separation because, when dissolving in water, sulfates are easily soluble, whereas oxides tend to be insoluble. The gas compositions of the two selected experimental conditions are presented in Table 2. For this study, sulfation roasting experiments were performed in these two conditions with and without the pre-roasting step for carbon removal.

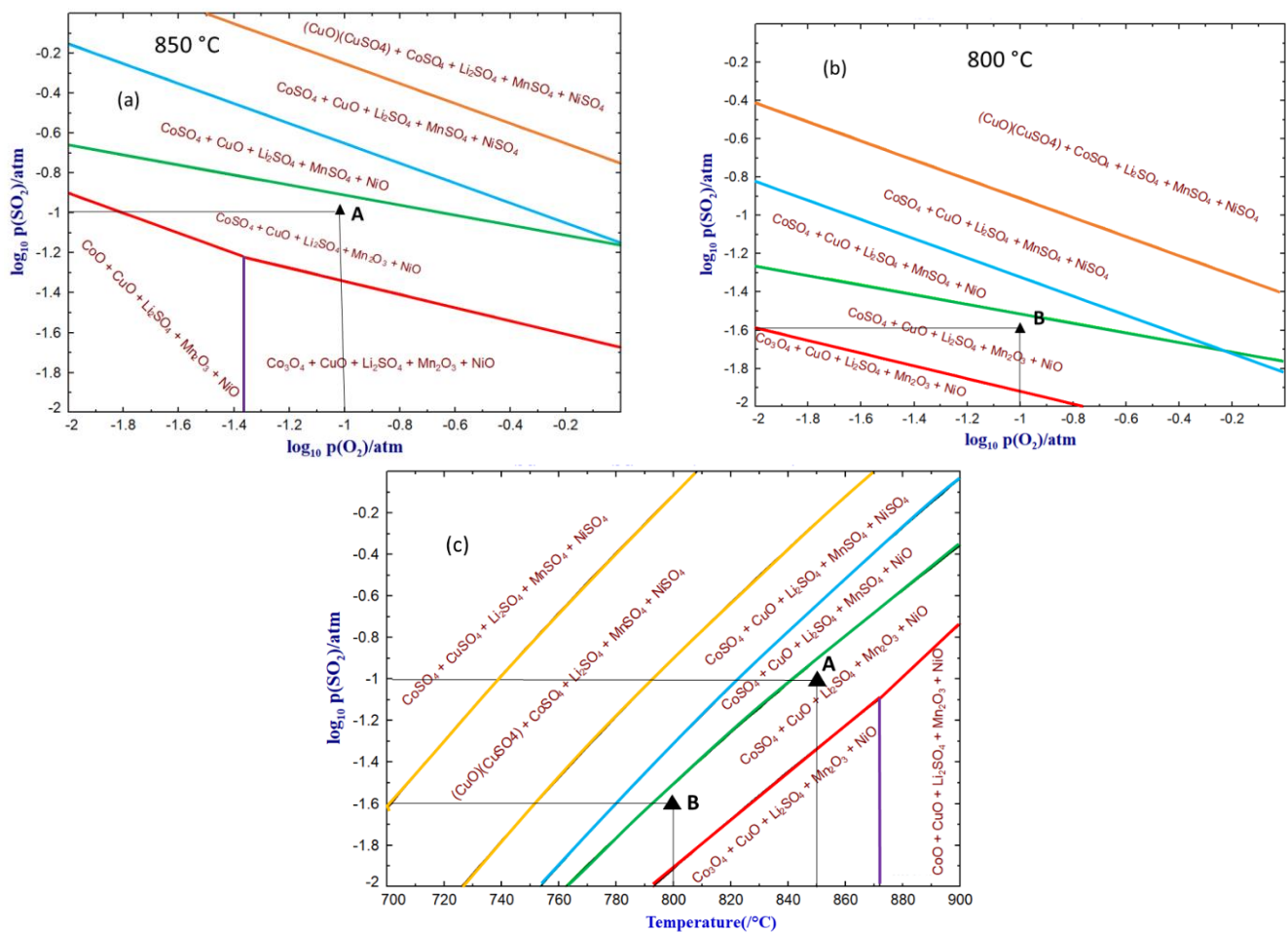


**Figure 5.** Thermodynamic stability diagram for Co-Li-Ni-Cu-Mn-S-O system (a) at 850 °C, (b) 800 °C, and (c) Variation in stability of phases with temperature and  $p_{SO_2}$  at  $p_{O_2}$  0.1 atm obtained from FactSage.

**Table 2.** Sulfation roasting conditions from stability analysis.

Conditions	Gas Composition	Temperature
A	10% $SO_2$ -10% $O_2$ -Ar	850 °C
B	2.5% $SO_2$ -10% $O_2$ -Ar	800 °C

### 3.3. Sulfation Roasting and Leaching

#### 3.3.1. With Carbon (Type 1)

Sulfation roasting experiments were performed with black mass for one hour under two temperature conditions—A and B, meaning 850 °C and 800 °C, respectively. This black mass contained graphite from the anode when sulfation roasting was performed. Thereafter, the sulfation roasted samples were leached into the water. The leached solution was filtered to separate the residue, which was digested into acids separately. Atomic absorption analysis (AAS) was conducted to measure the dissolved metal ion concentrations in the water-leached and residue-digested solution. The efficiency of the extraction of metals into the water-leached solution was calculated according to Equation (1); the analysis is presented in Table 3. To check the reproducibility, sulfation roasting experiments under condition A was repeated, and the extraction efficiency results were obtained within  $\pm 5\%$ .

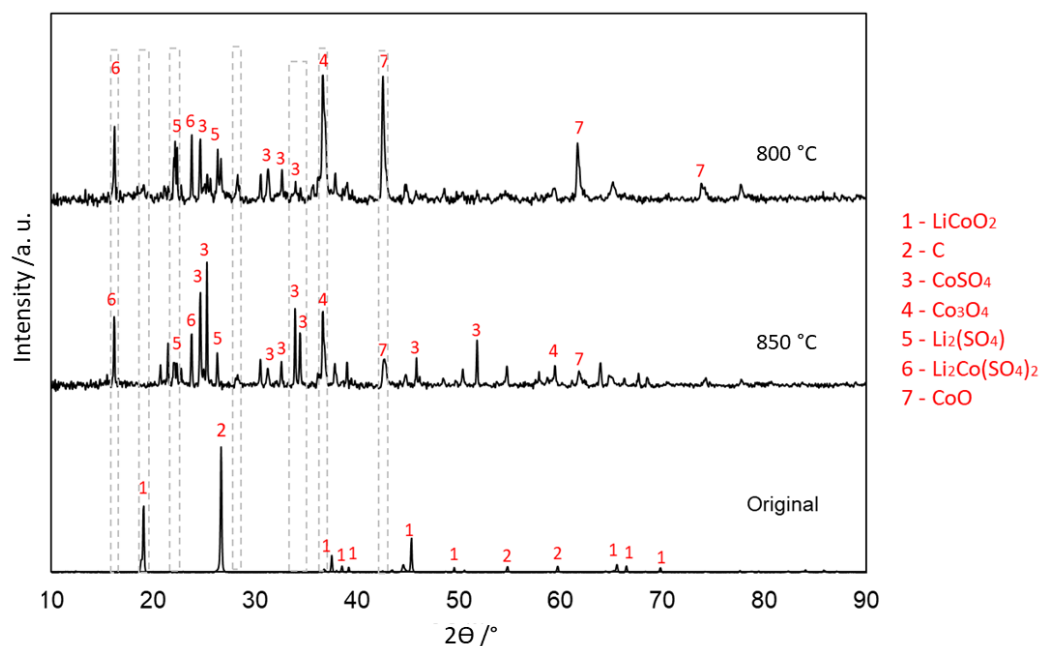


**Table 3.** Efficiency of extraction of metals into water in percentage (%) of 60 min sulfation roasted samples.

Conditions	Co (%)	Ni (%)	Mn (%)	Cu (%)	Fe (%)	Li (%)
A	61.21	22.99	68.36	24.53	0.00	99.51
B	24.02	11.15	26.57	1.72	0.00	91.75

The results presented in Table 3 show that it was possible to extract almost 61.21% of Co and 99.51% of Li by sulfation roasting with a gas mixture of 10% SO<sub>2</sub>-10% O<sub>2</sub>-Ar at 850 °C and subsequent water leaching. These results show that the rate of formation of sulfates rose with increasing sulfation roasting temperature, hence the higher extraction efficiency in condition A compared to B. It is interesting to note that, with increasing temperature, the rate of formation of all sulfates increases to varying degrees. It is worth mentioning that not only was there a sulfate formation of Co and Li, but other metals such as Ni, Mn, and Cu partly formed sulfates. This is not in agreement with the prediction from the thermodynamic stability diagram, which suggests that the impurities in the black mass would modify the thermodynamic conditions. Consequently, this result emphasizes the importance of studying real battery scrap instead of synthesized materials.

The comparison of XRD patterns in Figure 6 shows that the graphite/carbon present in the spent black mass disappears almost completely within 60 min of sulfation roasting. The profile also illustrates that the LiCoO<sub>2</sub> in the spent black mass either dissociates as its oxides or forms sulfates after 60 min of roasting time at both temperatures. The important sulfate phases are CoSO<sub>4</sub>, Li<sub>2</sub>Co(SO<sub>4</sub>)<sub>2</sub>, and Li<sub>2</sub>SO<sub>4</sub>. It can be observed that the CoSO<sub>4</sub> peaks are stronger at 850 °C in comparison to the intensity at 800 °C, whereas the intensity of the cobalt oxide (CoO and Co<sub>3</sub>O<sub>4</sub>) peaks is stronger at the lower temperature compared to that of higher temperature patterns. This suggests that, at the higher temperature, more Co transforms into sulfates, resulting in higher extraction efficiency, as presented in Table 3, and at the lower temperature, cobalt remained in oxide form. The diagram also shows that the intensity of the Li<sub>2</sub>SO<sub>4</sub> peak is stronger at 800 °C in comparison with the peak at 850 °C. However, the extraction efficiency of Li was observed to be higher at a higher temperature, and this could be illustrated due to the formation of Li<sub>2</sub>Co(SO<sub>4</sub>)<sub>2</sub> compounds.

**Figure 6.** XRD pattern of 60 min sulfation roasted samples in comparison with spent black mass.

### 3.3.2. Without Carbon (Type 2)

Another set of sulfation roasting experiments was conducted under similar experimental conditions (A and B), as mentioned in Table 2, after performing two stages of pre-roasting to facilitate the removal of graphite as well as some organic binders, plastics, and remaining electrolytes. Thereafter, the sulfation roasted samples were leached into the water, as described in Section 3.3.1. The water-leached and residue-digested solutions were analyzed in a similar way, and the metal extraction efficiency is presented in Table 4. The most interesting observation from this investigation is that the extraction efficiency decreased dramatically from 61.21% to 24.34% as a result of the additional pre-roasting stage. The selectivity (indicated as purity) of Co also decreased from 81% to 47%, where purity was defined as

$$\text{Co Purity} = \frac{m_{\text{Co}}}{m_{\text{Co}} + m_{\text{Li}} + m_{\text{Ni}} + m_{\text{Mn}} + m_{\text{Cu}}} \times 100\% \quad (2)$$

where  $m_i$  is the concentration of the dissolved metal  $i$  into the water in mg/L. This result reiterates the trend of the sulfation of Co and other metals with increasing temperature, as found in the case of sulfation roasting in the presence of carbon and other impurities.

**Table 4.** Percentage (%) of extraction metal ions into water-leached solution of 60 min sulfation roasted samples with two additional pre-roasting stages.

Conditions	Co (%)	Ni (%)	Mn (%)	Cu (%)	Fe (%)	Li (%)
A	24.34	33.00	46.61	21.60	0.00	88.75
B	17.41	17.22	26.52	6.87	0.00	88.99

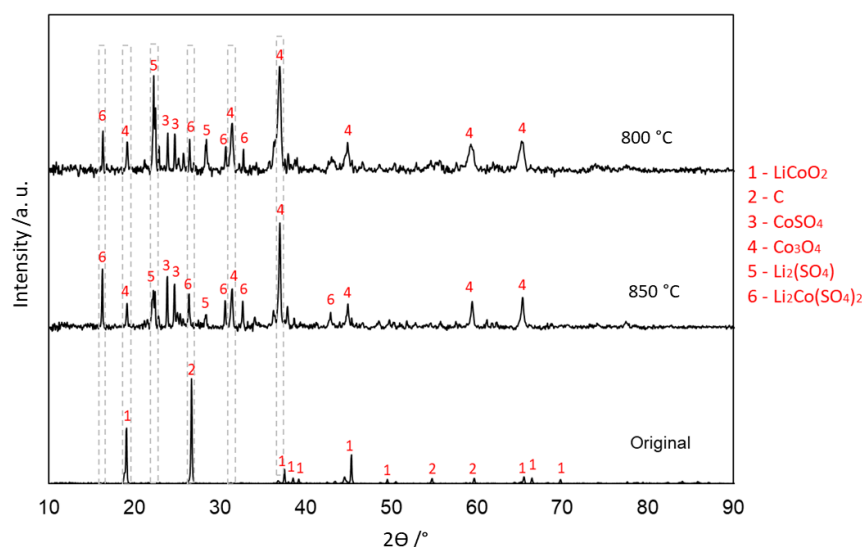
It is evident from the XRD patterns of the two-stage pre-roasted and 60 min sulfation roasted samples shown in Figure 7 that the carbon peak disappeared for both 800 °C and 850 °C. Similarly to the previous case, LiCoO<sub>2</sub> either dissociated into oxides or formed sulfates such as Li<sub>2</sub>Co(SO<sub>4</sub>)<sub>2</sub>, CoSO<sub>4</sub>, and Li<sub>2</sub>SO<sub>4</sub>. The peak intensity of Li<sub>2</sub>SO<sub>4</sub> was higher for the lower temperature, which is in agreement with the previous observation made in Section 3.3.1. The intensity of the CoSO<sub>4</sub> peaks is comparatively stronger for the higher temperature. Additionally, a comparison of the Li<sub>2</sub>Co(SO<sub>4</sub>)<sub>2</sub> peak intensities at the two different temperatures demonstrates that the intensity was higher at 850 °C than at 800 °C. This illustrates that a higher extraction efficiency of Li and Co takes place at a higher temperature. This trend was also observed when sulfation roasting was performed with carbon in SO<sub>2</sub>-O<sub>2</sub>-Ar gas at similar temperatures. The comparison of the intensity of the CoSO<sub>4</sub> peaks of sulfation-roasted samples with and without carbon at 850 °C showed that the intensity was very strong in the presence of carbon. In contrast, the Co<sub>3</sub>O<sub>4</sub> peak was very strong at 850 °C when pre-roasting was conducted before sulfation roasting. This demonstrates additional evidence of the higher extraction efficiency of Co for sulfation roasting in the presence of carbon. Additionally, it could be noticed that, in the current case, mainly Co<sub>3</sub>O<sub>4</sub> peaks were dominant, whereas CoO peaks were also strongly present when sulfation roasting was performed with carbon.

### 3.4. Evolution of Phases in Sulfation Roasting

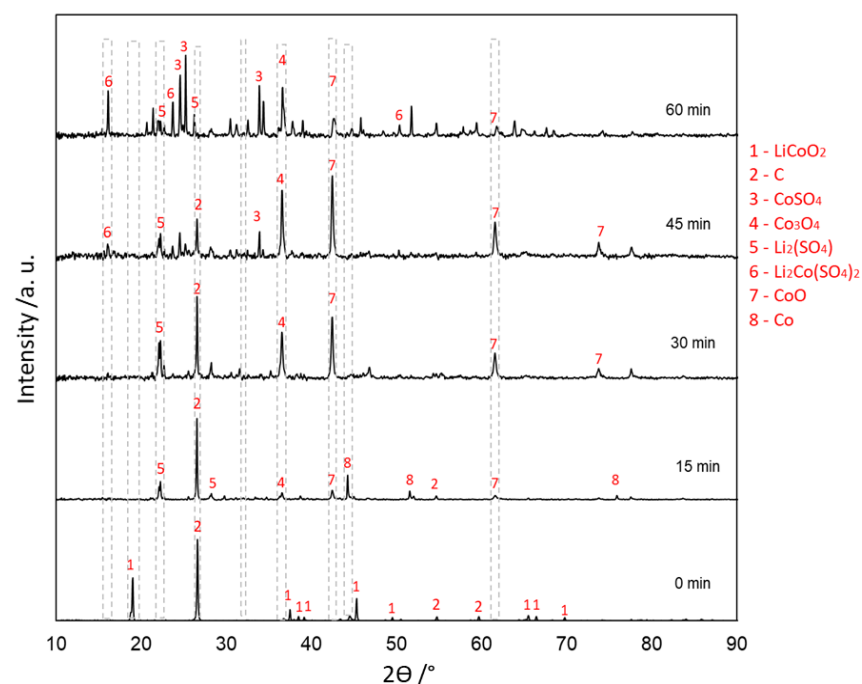
#### 3.4.1. With Carbon (Type 1)

As discussed in Section 3.3, the presence of carbon and other impurities in the spent black mass enhances the efficiency of Co extraction from the black mass. To further investigate the underlying mechanism, sulfation roasted samples were collected after 15 min, 30 min, 45 min, and 60 min at 850 °C with 10% SO<sub>2</sub>, 10% O<sub>2</sub>, and 80% Ar gas composition (condition A). The XRD pattern and SEM-EDS composition mapping were analyzed for these samples and are presented in Figures 8 and 9. It can be observed in Figure 8 that the intensity of the characteristic carbon peak at 26.6° decreased with the

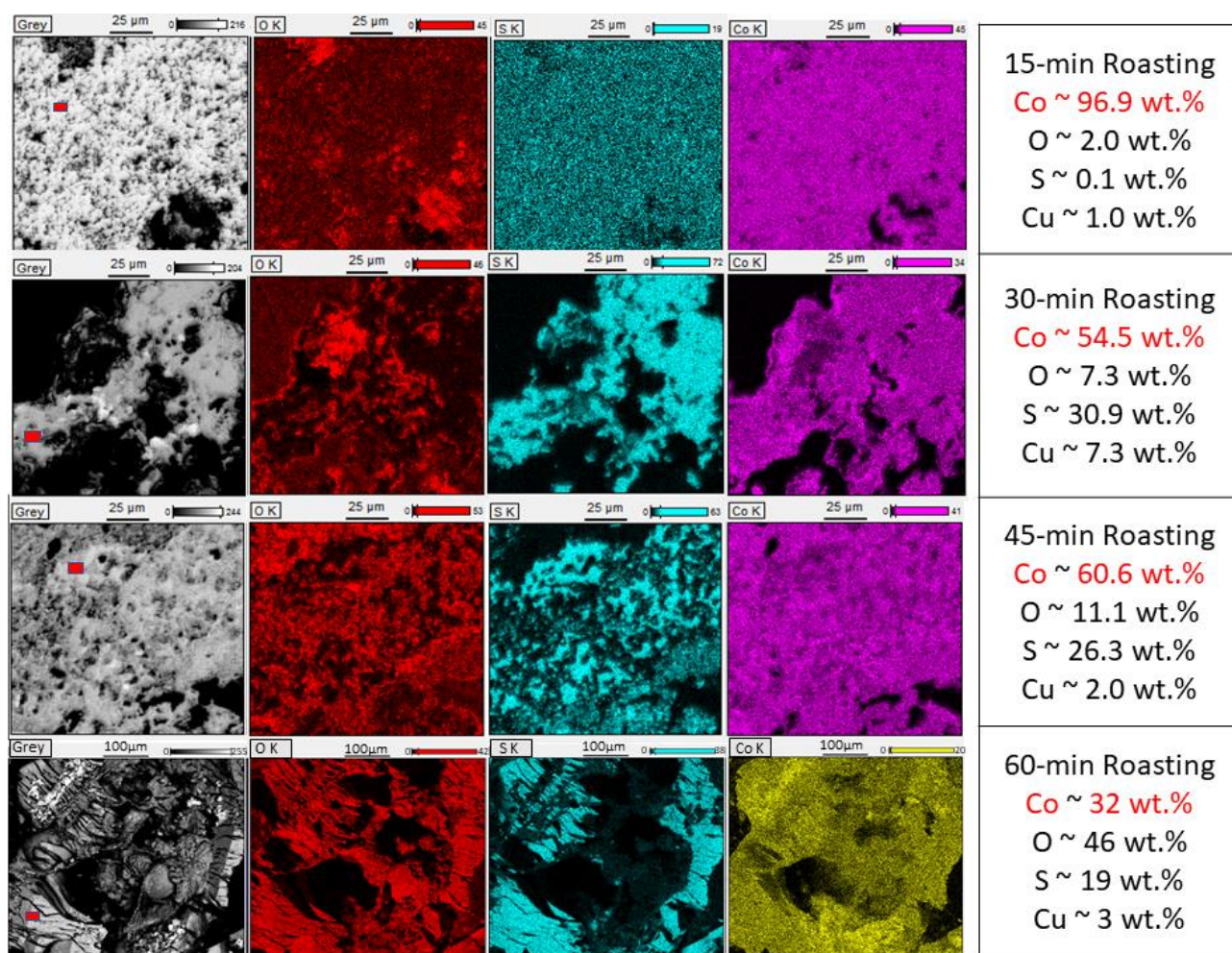
progression of the reaction and almost disappeared in the pattern for 45 min for the roasted samples. Within 15 min,  $\text{LiCoO}_2$  had dissociated completely, and no peaks of this oxide were present in the XRD patterns for samples roasted for 15 min and longer. It is interesting to note in Figure 8 that the  $\text{Li}_2\text{SO}_4$  peak is prominent in the pattern for 15 min sulfation roasted samples, whereas it diminishes slowly as roasting progresses. In contrast, the  $\text{Li}_2\text{Co}(\text{SO}_4)_2$  peak appears stronger from 15 min to 60 min of roasting. In the pattern for 15 min samples, it could be observed that the metallic cobalt (Co) phase was present: the cobalt sulfate or cobalt oxide phases appeared after 30 min of roasting and slowly became stronger with time, as shown in the 45 min and 60 min patterns. This suggests that, initially,  $\text{LiCoO}_2$  was reduced to metallic cobalt and later transformed into sulfate.



**Figure 7.** XRD pattern of 60 min sulfation roasted samples in comparison with spent black mass and additional pre-roasting.



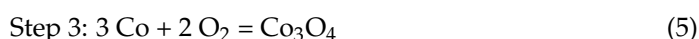
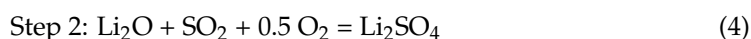
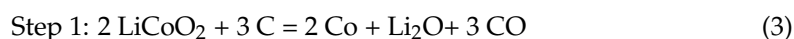
**Figure 8.** XRD pattern for 15-min, 30-min, 45-min, and 60 min sulfation roasted samples in the presence of carbon.



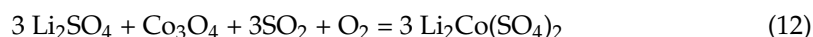
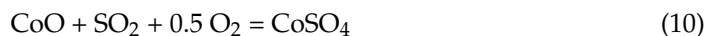
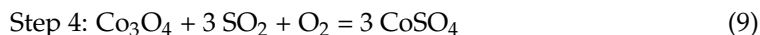
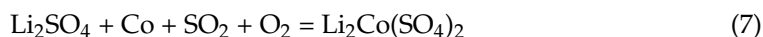
**Figure 9.** Composition mapping from SEM-EDS for 15-min, 30-min, 45-min, and 60 min sulfation roasted samples in the presence of carbon along with composition of the ‘red marked’ regions.

The SEM-EDS mapping shown in Figure 9 of the samples corresponding to those presented in Figure 8 shows that, after 15 min of sulfation roasting, metallic Co was formed. This agrees with the observation from XRD, confirming that all of the lithium cobalt oxides were reduced by carbon to metallic Co. It was not possible to detect lithium in SEM-EDS due to the low energy characteristic rays. A comparison of the composition mapping and the point analysis for 30-min, 45-min, and 60 min samples showed that the samples were enriched with oxygen and sulfur over time. This also suggests that the metallic Co may have been going through a transition from a mixture of sulfates and oxides to cobalt sulfate after 60-min of sulfation roasting. When interpreting the composition mapping results, it is worth mentioning that the lithium sulfates might have contributed to the S and O analysis.

This investigation demonstrates that sulfate formation occurs through a sequence of four reaction steps. In the first step,  $\text{LiCoO}_2$  is reduced by carbon to metallic Co and possibly  $\text{Li}_2\text{O}$ ;  $\text{Li}_2\text{O}$  transformed rapidly into  $\text{Li}_2\text{SO}_4$ . As the transformation of the lithium sulfate is very fast, no  $\text{Li}_2\text{O}$  peak was observed in the XRD pattern of the 15 min roasted samples. Therefore, this intermediate phase of Li could be considered a hypothesis.







Then, the major fraction of metallic Co transforms into either cobalt oxides (CoO and  $\text{Co}_3\text{O}_4$ ) or a cobalt sulfate, and a small fraction of the metallic Co forms a compound sulfate ( $\text{Li}_2\text{Co}(\text{SO}_4)_2$ ) by reacting with  $\text{Li}_2\text{SO}_4$ ,  $\text{SO}_2$ , and  $\text{O}_2$ . These parallel transformations leave almost no metallic Co after 30 min of sulfation roasting. Finally, as the reaction proceeds, a fraction of the cobalt oxides transforms into sulfates or CoO, which further oxidizes, leaving unreacted  $\text{Co}_3\text{O}_4$ . Interestingly, the XRD pattern of 60 min sulfation roasted samples mainly exhibits the presence of  $\text{Co}_3\text{O}_4$ , whereas both the CoO and  $\text{Co}_3\text{O}_4$  phases exist in the XRD patterns of 30 min and 45 min samples. This leads to the hypothesis that the formation of cobalt sulfate occurred in the cobalt sulfate mainly from metallic Co or from CoO.

### 3.4.2. Without Carbon (Type 2)

As described earlier, sulfation roasting experiments were performed with additional pre-roasting (initially in argon for 2 h and in an Ar- $\text{O}_2$  mixture for 3 h) to burn the graphite present in the black mass before sulfation roasting. The extraction efficiency was observed to deteriorate due to the removal of carbon by pre-roasting before sulfation roasting. To distinguish the pathways of sulfate formation in the two different cases, similarly to the previous case, samples were collected for 15 min, 45 min, and 60 min of sulfation roasting after 5 h of pre-roasting. To understand the phase evolution, XRD patterns and SEM-EDS composition mapping were obtained for 15-min, 45-min, and 60-min sulfation roasted samples after pre-roasting, as presented in Figures 10 and 11.

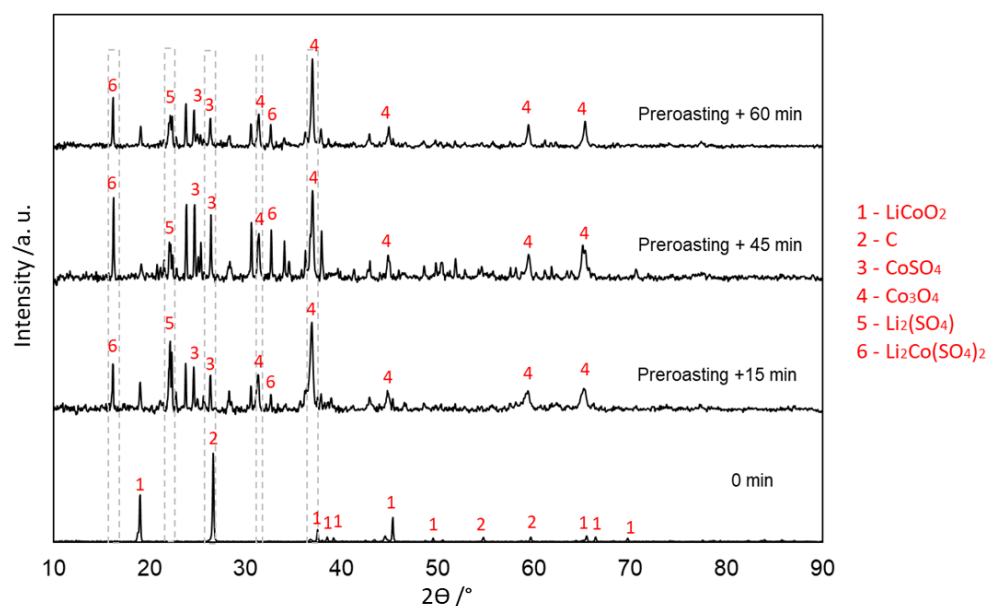


**Figure 10.** XRD pattern for 15-min, 45-min, and 60 min sulfation roasted samples with additional pre-roasting.



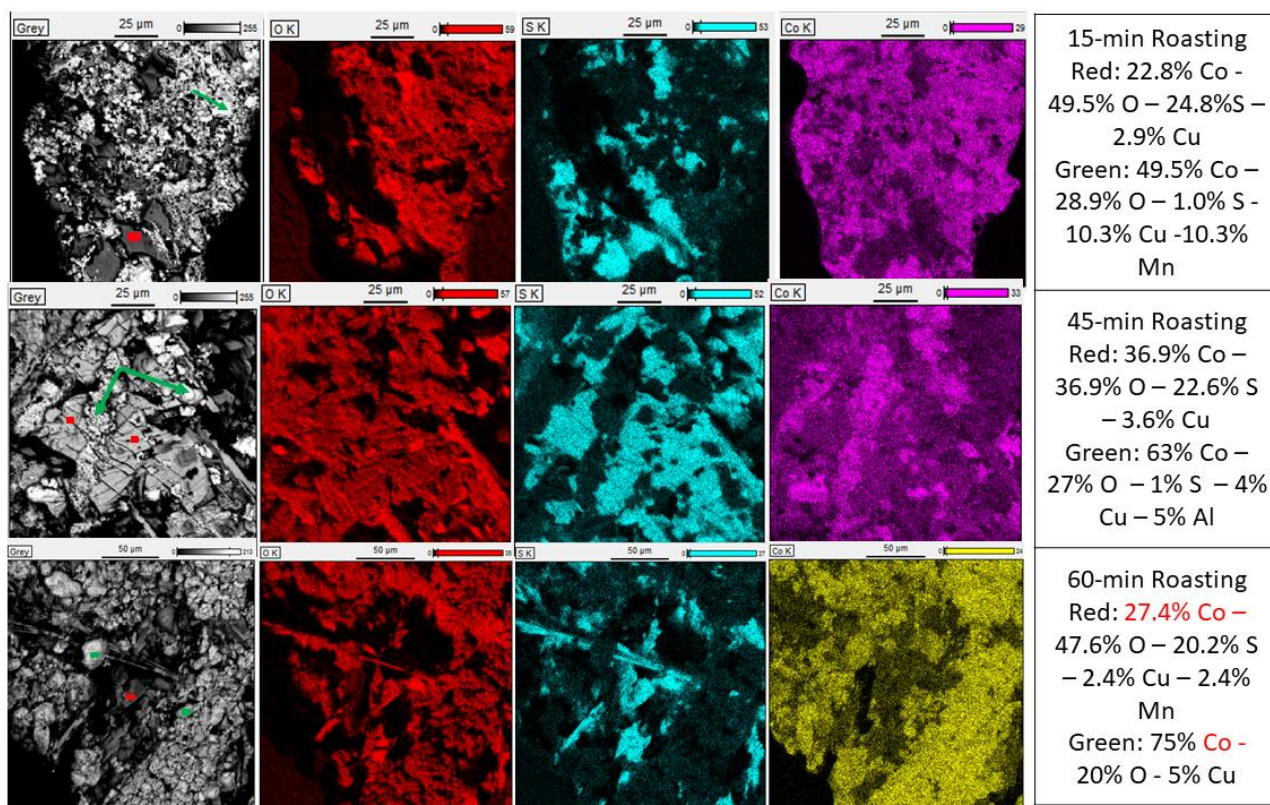
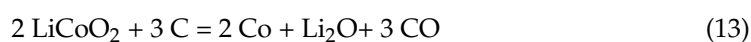


**Figure 11.** Composition mapping from SEM-EDS for 15-min, 45-min, and 60 min sulfation roasted samples with additional pre-roasting along with composition of the ‘red’ and ‘green’ marked regions.

It is evident from the pattern of the 15 min roasted samples that the carbon peak almost disappeared. Therefore, this establishes the fact that carbon removal was completed in the pre-roasting stage, and carbon had no effect on sulfation roasting. It is interesting to note that the  $\text{Co}_3\text{O}_4$  peak is very strong starting from 15 min, unlike the case when sulfation roasting was conducted in the presence of carbon, and this peak intensity remained strong until 60 min of roasting as well. Another interesting point here is that the  $\text{Li}_2\text{Co}(\text{SO}_4)_2$  peaks appear strongly in the 15 min sulfation roasted samples, whereas this peak was not so dominant initially when carbon was present during sulfation roasting. This peak became stronger as sulfation roasting progressed, and the  $\text{Li}_2\text{SO}_4$  peak became weaker over time. A similar pattern was observed in the previous case as well.

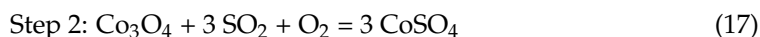
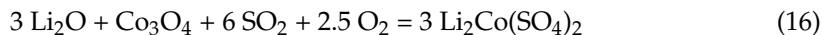
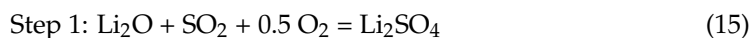
The composition mapping for the 15 min roasted sample, presented in Figure 11, illustrates that most metals existed either as oxides or sulfates; no metallic Co was present. The grayer islands marked by red points are of sulfates, and the shiny areas are oxides marked by green arrows. It is important to note that a significant amount of cobalt oxide was still present at the end of 60 min of sulfation roasting.

The analysis of composition mapping and the XRD pattern of sulfation roasted samples for different times after pre-roasting illustrates the sequence of phase formation, and a possible reaction pathway can be established. During pre-roasting, all of the lithium cobalt oxide dissociated into cobalt oxide and possibly into lithium oxide:



Within the initial 15 min of sulfation roasting, all of the lithium oxide transformed into mostly lithium sulfate and some small fraction into  $\text{Li}_2\text{Co}(\text{SO}_4)_2$ . In later stages, a fraction of  $\text{Co}_3\text{O}_4$  transforms into  $\text{Li}_2\text{Co}(\text{SO}_4)_2$  or  $\text{CoSO}_4$ . However, a significant amount of cobalt

oxide ( $\text{Co}_3\text{O}_4$ ) remained untransformed until 60 min of sulfation roasting. The steps of sulfation roasting are described here as follows:



The main difference between the reaction trajectory of sulfate formation with and without pre-roasting is the formation of metallic cobalt and  $\text{CoO}$  and, consequently, the formation of sulfates from these phases. Instead of this step, when pre-roasting was conducted, the  $\text{Co}_3\text{O}_4$  phase was dominant from a very early period, and cobalt sulfate was formed from  $\text{Co}_3\text{O}_4$ . This  $\text{Co}_3\text{O}_4$  phase could possibly hinder further transformation into sulfates and result in very low Co recovery in this case.

### 3.5. Extraction of Co and Li into Water after Roasting

The investigation of sulfation roasting without pre-roasting and with two stages of pre-roasting suggests that the presence of carbon is beneficial for the selective extraction of Co. A higher temperature also enhances the kinetics of sulfate formation. Therefore, the variation in yield of Co and Li and other metals extraction over time was measured for sulfation roasting in the presence of carbon under 'A' conditions, i.e., 10%  $\text{SO}_2$ -10%  $\text{O}_2$ -Ar gas at 850 °C, as presented in Figure 12.

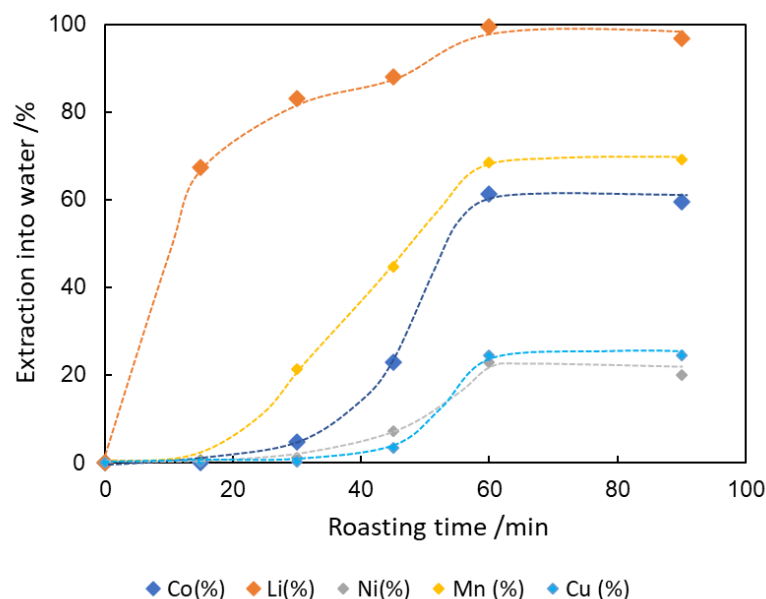


**Figure 12.** Extraction (%) of metals into water as a function of roasting time from black mass by sulfation roasting with 10%  $\text{SO}_2$ -10%  $\text{O}_2$ -Ar gas at 850 °C in the presence of carbon.

According to the thermodynamic stability diagram shown in Figure 5, the formation of lithium sulfate was unavoidable, and this is reflected in the lithium extraction yield, as almost 99.51% of the lithium was recovered. This also demonstrates that Co extraction is almost complete within 60 min of sulfation roasting, and a maximum of 61.21% of Co can be extracted by this sulfation roasting technique from industrial LIB scrap. A Co purity of 81% was obtained, in this case, with a maximum extraction efficiency of 61.21%. In a previous study [43] carried out in the authors' laboratory with synthetic  $\text{LiCoO}_2$  powder, only 17.4% Co could be recovered by this sulfation roasting technique, whereas this study using industrial battery scrap demonstrated a much higher Co extraction efficiency. However,

the extraction efficiency is lower than the efficiency reported from hydrometallurgical extraction routes. Most of the hydrometallurgical research on metal recovery involves acid leaching [9,11–15], reductive acid leaching [10,11,16], or a combination of thermal pretreatment and leaching [18,19] followed by metal separation steps such as solvent extraction, precipitation, etc., achieving an extraction efficiency as high as 90% from these routes. The main drawback of the hydrometallurgy route is the consumption of a high volume of acids. Moreover, industrial pyrometallurgical routes such as the smelting experience loss of Li in the fumes or in the slag and are highly energy intensive. The proposed route is a medium-temperature process that avoids the consumption of acids, and in addition, the recovery rate of Li is very high. However, further investigation is needed to improve the cobalt recovery and, if possible, as well as the recovery of graphite. In addition to Li and Co recovery, Figure 12 also shows the recovery of 70% Mn, 25% Cu, and 20% Ni. This also indicates that the rate of formation of the sulfate is highest for Li compared to other metals.

The comparison of the reaction pathways of sulfation reaction with and without the presence of carbon suggests that the cobalt sulfate formation kinetics from metallic cobalt or CoO is faster in comparison with the formation of sulfates from  $\text{Co}_3\text{O}_4$ . In the case of sulfation roasting in the presence of carbon,  $\text{Co}_3\text{O}_4$  formation occurred during the later stages of the reaction (30 min onwards), and this phase may have hindered further sulfation. However, in the case of sulfation roasting without carbon, from a very early stage, cobalt was present as  $\text{Co}_3\text{O}_4$ , and the sulfation of cobalt became even slower, which is illustrated in Table 4. The Gibbs free energy of the formation of the cobalt sulfate from metallic Co and cobalt oxides (CoO and  $\text{Co}_3\text{O}_4$ ), presented in Figure 13 (using HSC software, version 10.0.8.5), suggests a higher thermodynamic driving force for the formation of cobalt sulfate from metallic Co.

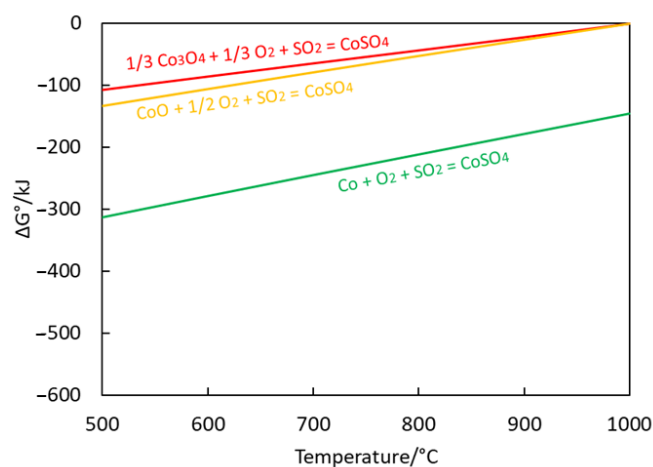


**Figure 13.** Gibbs free energy formation of cobalt sulfate from metallic cobalt and cobalt oxides.

Another possible reason could be the diffusion limitation of cobalt ions in the cobalt oxide phases. Carbon may have delayed the formation of cobalt oxides, and, therefore, a higher recovery of Co was observed. Currently, we are unable to present proper evidence for this type of kinetic barrier. Further investigation in our laboratory is being carried out to understand the kinetics in detail.

#### 4. Conclusions

The combination of selective sulfation roasting and water leaching is a potential metal recovery process from complex mixtures of metals such as battery scrap. In this work, sulfation roasting with water leaching methodology was investigated for extracting Co and Li selectively from spent black mass. A significant fraction of graphite in the spent black mass comes from the anode, and its presence during sulfation roasting was found to be beneficial for Co extraction. The sulfate formation pathways were compared for

samples after sulfation roasting with and without the presence of carbon. It was found that  $\text{LiCoO}_2$  initially formed metallic Co in sulfation roasting with carbon for samples roasted for 15 min, whereas  $\text{Co}_3\text{O}_4$  was formed when pre-roasting was performed before sulfation roasting. Then, sulfates were formed in the subsequent reaction stages. For the best experimental conditions, i.e., sulfation roasting at 850 °C under a gas flow of 10%  $\text{SO}_2$ -10%  $\text{O}_2$ -Ar, the maximum extraction of Co was possible within 60 min of roasting in the presence of carbon. The maximum extraction efficiency obtained with this method was 99.51% for Li and 61.21% for Co, which is much higher than the reported extraction efficiency (17.4% Co) from a previous study [43] by this route. The main advantage of the proposed route is that the consumption of hazardous acids could be avoided, whereas acids are an essential component in hydrometallurgical processing. This process also shows the significant recovery of Li, which is typically lost in other high-temperature processes such as smelting. From this study, it can be concluded that, although Co and Li could be extracted from the black mass by this technique, it is not as selective as pure thermodynamics suggests. Furthermore, the presence of impurities and the complex nature of the materials destroy the selectivity of elements for sulfation. Further investigation, such as the incorporation of catalysts to enhance the sulfation kinetics, the effect of particle size, or testing a combination of unit processes, is needed to improve Co extraction efficiency.

**Author Contributions:** Conceptualization, J.B., S.U., X.W. and A.J.; data curation, J.B., S.U. and J.P.; formal analysis, J.B. and S.U.; funding acquisition, A.J.; investigation, J.B. and S.U.; methodology, J.B. and S.U.; project administration, M.L. and A.J.; resources, M.L. and A.J.; supervision, M.L. and A.J.; validation, J.B. and S.U. and A.J.; writing—original draft, J.B.; writing—review and editing, M.L. and A.J. All authors have read and agreed to the published version of the manuscript.

**Funding:** This research was funded by the Academy of Finland in the GOVERMAT project (Grant no. 346728).

**Data Availability Statement:** Not applicable.

**Acknowledgments:** The authors are grateful to Akkuser Oy (Finland) for providing the battery scrap. The authors would like to thank Lassi Klemettinen and Anna Klemettinen for their training on working with the furnace and SEM. The authors are also grateful to the Academy of Finland for providing financial support for this project (GOVERMAT, grant 346728). This study utilized the Academy of Finland's RawMatTERS Finland Infrastructure (RAMI), based jointly at Aalto University, GTK Espoo, and VTT Espoo.

**Conflicts of Interest:** The authors declare no conflict of interest.

## References

1. Roper, W. High Demand for Lithium-Ion Batteries Statista. Available online: <https://www.statista.com/chart/23808/lithium-ion-battery-demand/> (accessed on 15 July 2022).
2. Zhang, W.; Xu, C.; He, W.; Li, G.; Huang, J. A review on management of spent lithium-ion batteries and strategy for resource recycling of all components from them. *Waste Manag. Res.* **2018**, *36*, 99–112. [CrossRef] [PubMed]
3. Neumann, J.; Petranikova, M.; Meeus, M.; Gamarra, J.; Younesi, R.; Winter, M.; Nowak, S. Recycling of Lithium-Ion Batteries—Current State of the Art, Circular Economy, and Next Generation Recycling. *Adv. Energy Mater.* **2022**, *12*, 2102917. [CrossRef]
4. Kamczyc Alex: New Research Shows Boom in End-of-Life Lithium-Ion Batteries—Recycling Today. Available online: <https://www.recyclingtoday.com/article/lux-research-sees-boon-in-lithium-ion-battery-end-markets/> (accessed on 15 July 2022).
5. Zhao, Y.; Pohl, O.; Bhatt, A.; Collis, G.; Mahon, P.; Rüther, T.; Hollenkamp, A.F. A Review on Battery Market Trends, Second-Life Reuse, and Recycling. *Sustain. Chem.* **2021**, *2*, 167–205. [CrossRef]
6. Lithium-ion Battery Market Size Worth \$182.53 Billion By 2030: Grand View Research, Inc.—Bloomberg. Available online: <https://www.bloomberg.com/press-releases/2022-06-07/lithium-ion-battery-market-size-worth-182-53-billion-by-2030-grand-view-research-inc> (accessed on 13 November 2022).
7. Woollacott, E. Electric Cars: What will Happen to All the Dead Batteries?—BBC News. Available online: <https://www.bbc.com/news/business-56574779> (accessed on 22 September 2022).
8. REPORT on the Proposal for a Regulation of the European Parliament and of the Council Concerning Batteries and Waste Batteries, Repealing Directive 2006/66/EC and Amending Regulation (EU) No. 2019/1020 | A9-0031/2022. European Parliament. Available online: [https://www.europarl.europa.eu/doceo/document/A-9-2022-0031\\_EN.html](https://www.europarl.europa.eu/doceo/document/A-9-2022-0031_EN.html) (accessed on 7 October 2022).



9. Lee, J.-J.; Chung, J.-D. A study on the cobalt and lithium recovery from the production scraps of lithium secondary battery by high efficient and eco-friendly method. *J. Korean Inst. Resour. Recycl.* **2010**, *19*, 51–60.
10. Peng, C.; Hamuyuni, J.; Wilson, B.; Lundström, M. Selective reductive leaching of cobalt and lithium from industrially crushed waste Li-ion batteries in sulfuric acid system. *Waste Manag.* **2018**, *76*, 582–590. [[CrossRef](#)]
11. Chen, X.; Chen, Y.; Zhou, T.; Liu, D.; Hu, H.; Fan, S. Hydrometallurgical recovery of metal values from sulfuric acid leaching liquor of spent lithium-ion batteries. *Waste Manag.* **2015**, *38*, 349–356. [[CrossRef](#)]
12. Guo, Y.; Li, F.; Zhu, H.; Li, G.; Huang, J.; He, W. Leaching lithium from the anode electrode materials of spent lithium-ion batteries by hydrochloric acid (HCl). *Waste Manag.* **2016**, *51*, 227–233. [[CrossRef](#)]
13. Chen, X.; Ma, H.; Luo, C.; Zhou, T. Recovery of valuable metals from waste cathode materials of spent lithium-ion batteries using mild phosphoric acid. *J. Hazard. Mater.* **2017**, *326*, 77–86. [[CrossRef](#)]
14. Meshram, P.; Pandey, B.; Mankhand, T. Recovery of valuable metals from cathodic active material of spent lithium ion batteries: Leaching and kinetic aspects. *Waste Manag.* **2015**, *45*, 306–313. [[CrossRef](#)]
15. Ma, L.; Nie, Z.; Xi, X.; Han, X. Cobalt recovery from cobalt-bearing waste in sulphuric and citric acid systems. *Hydrometallurgy* **2013**, *136*, 1–7. [[CrossRef](#)]
16. Pagnanelli, F.; Moscardini, E.; Altimari, P.; Atia, T.A.; Toro, L. Cobalt products from real waste fractions of end of life lithium ion batteries. *Waste Manag.* **2016**, *51*, 214–221. [[CrossRef](#)]
17. Lombardo, G.; Ebin, B.; Foreman, M.S.; Steenari, B.; Petranikova, M. Incineration of EV Lithium-ion batteries as a pretreatment for recycling—Determination of the potential formation of hazardous by-products and effects on metal compounds. *ACS Sustain. Chem. Eng.* **2019**, *7*, 13668–13679. [[CrossRef](#)]
18. Yang, Y.; Huang, G.; Xu, S.; He, Y.; Liu, X. Thermal treatment process for the recovery of valuable metals from spent lithium-ion batteries. *Hydrometallurgy* **2016**, *165*, 390–396. [[CrossRef](#)]
19. Pavón, S.; Kahl, M.; Hippmann, S.; Bertau, M. Lithium recovery from production waste by thermal pre-treatment. *Sustain. Chem. Pharm.* **2022**, *28*, 100725. [[CrossRef](#)]
20. Rinne, M.; Elomaa, H.; Porvali, A.; Lundström, M. Simulation-based life cycle assessment for hydrometallurgical recycling of mixed LIB and NiMH waste. *Resour. Conserv. Recycl.* **2021**, *170*, 105586. [[CrossRef](#)]
21. Li, J.; Wang, G.; Xu, Z. Environmentally-friendly oxygen-free roasting/wet magnetic separation technology for in situ recycling cobalt, lithium carbonate and graphite from spent LiCoO<sub>2</sub>/graphite lithium batteries. *J. Hazard. Mater.* **2016**, *302*, 97–104. [[CrossRef](#)]
22. Zhang, J.; Hu, J.; Zhang, W.; Chen, Y.; Wang, C. Efficient and economical recovery of lithium, cobalt, nickel, manganese from cathode scrap of spent lithium-ion batteries. *J. Clean Prod.* **2018**, *204*, 437–446. [[CrossRef](#)]
23. Hu, J.; Zhang, J.; Li, H.; Chen, Y.; Wang, C. A promising approach for the recovery of high value-added metals from spent lithium-ion batteries. *J. Power Sources* **2017**, *351*, 192–199. [[CrossRef](#)]
24. Liu, P.; Xiao, L.; Tang, Y.; Chen, Y.; Ye, L.; Zhu, Y. Study on the reduction roasting of spent LiNi<sub>x</sub>Co<sub>y</sub>Mn<sub>z</sub>O<sub>2</sub> lithium-ion battery cathode materials. *J. Therm. Anal. Calorim.* **2019**, *136*, 1323–1332. [[CrossRef](#)]
25. Ma, Y.; Tang, J.; Wanaldi, R.; Zhou, X.; Wang, H.; Zhou, C.; Yang, J. A promising selective recovery process of valuable metals from spent lithium ion batteries via reduction roasting and ammonia leaching. *J. Hazard. Mater.* **2021**, *402*, 123491. [[CrossRef](#)] [[PubMed](#)]
26. Tang, Y.; Xie, H.; Zhang, B.; Chen, X.; Zhao, Z.; Qu, J.; Xing, P.; Yin, H. Recovery and regeneration of LiCoO<sub>2</sub>-based spent lithium-ion batteries by a carbothermic reduction vacuum pyrolysis approach: Controlling the recovery of CoO or Co. *Waste Manag.* **2019**, *97*, 140–148. [[CrossRef](#)] [[PubMed](#)]
27. Xiao, J.; Li, J.; Xu, Z. Recycling metals from lithium ion battery by mechanical separation and vacuum metallurgy. *J. Hazard. Mater.* **2017**, *338*, 124–131. [[CrossRef](#)] [[PubMed](#)]
28. Peng, Q.; Zhu, X.; Li, J.; Liao, Q.; Lai, Y.; Zhang, L.; Fu, Q.; Zhu, X. A novel method for carbon removal and valuable metal recovery by incorporating steam into the reduction-roasting process of spent lithium-ion batteries. *Waste Manag.* **2021**, *134*, 100–109. [[CrossRef](#)] [[PubMed](#)]
29. Wang, W.; Zhang, Y.; Zhang, L.; Xu, S. Cleaner recycling of cathode material by in-situ thermite reduction. *J. Clean Prod.* **2020**, *249*, 119340. [[CrossRef](#)]
30. Wang, W.; Zhang, Y.; Liu, X.; Xu, S. A Simplified Process for Recovery of Li and Co from Spent LiCoO<sub>2</sub> Cathode Using Al Foil as the in situ Reductant. *ACS Sustain. Chem. Eng.* **2019**, *7*, 12222–12230. [[CrossRef](#)]
31. Ren, G.; Xiao, S.; Xie, M.; Pan, B.; Chen, J.; Wang, F.; Xia, X. Recovery of valuable metals from spent lithium ion batteries by smelting reduction process based on FeO–SiO<sub>2</sub>–Al<sub>2</sub>O<sub>3</sub> slag system. *Trans. Nonferrous Met. Soc. China* **2017**, *27*, 450–456. [[CrossRef](#)]
32. Sommerfeld, M.; Hovestadt, G.; Friedrich, B. Smelting of Pyrolyzed Lithium-Ion Battery Black Mass using a Calcium-Aluminate Slag System. In Proceedings of the European Metallurgical Conference (EMC) 2021, Salzburg, Germany, 27 June 2021.
33. Sommerfeld, M.; Vonderstein, C.; Dertmann, C.; Klimko, J.; Oráč, D.; Mišuková, A.; Havlík, T.; Friedrich, B. A Combined Pyro- and Hydrometallurgical Approach to Recycle Pyrolyzed Lithium-Ion Battery Black Mass Part 1: Production of Lithium Concentrates in an Electric Arc Furnace. *Metals* **2020**, *10*, 1069. [[CrossRef](#)]
34. Cheret, D.; Santén, S. Battery Recycling. European Patent 1589121B1, 26 October 2005.
35. Velázquez-Martínez, O.; Valio, J.; Santasalo-Aarnio, A.; Reuter, M.; Serna-Guerrero, R. A Critical Review of Lithium-Ion Battery Recycling Processes from a Circular Economy Perspective. *Batteries* **2019**, *5*, 5. [[CrossRef](#)]



36. Harper, G.; Sommerville, R.; Kendrick, E.; Driscoll, L.; Slater, P.; Stolkin, R.; Walton, A.; Christensen, P.; Heidrich, O.; Lambert, S.; et al. Recycling lithium-ion batteries from electric vehicles. *Nature* **2019**, *575*, 575. [\[CrossRef\]](#)
37. Makuza, B.; Tian, Q.; Guo, X.; Chattopadhyay, K.; Yu, D. Pyrometallurgical options for recycling spent lithium-ion batteries: A comprehensive review. *J. Power Sources* **2021**, *491*, 229622. [\[CrossRef\]](#)
38. Fan, E.; Li, L.; Lin, J.; Wu, J.; Yang, J.; Wu, F.; Chen, R. Low-Temperature Molten-Salt-Assisted Recovery of Valuable Metals from Spent Lithium-Ion Batteries. *ACS Sustain. Chem. Eng.* **2019**, *7*, 16144–16150. [\[CrossRef\]](#)
39. Barrios, O.; González, Y.; Barbosa, L.; Orosco, P. Chlorination roasting of the cathode material contained in spent lithium-ion batteries to recover lithium, manganese, nickel and cobalt. *Miner. Eng.* **2022**, *176*, 107321. [\[CrossRef\]](#)
40. Qu, X.; Xie, H.; Chen, X.; Tang, Y.; Zhang, B.; Xing, P.; Yin, H. Recovery of LiCoO<sub>2</sub> from Spent Lithium-Ion Batteries through a Low-Temperature Ammonium Chloride Roasting Approach: Thermodynamics and Reaction Mechanisms. *ACS Sustain. Chem. Eng.* **2020**, *8*, 6524–6532. [\[CrossRef\]](#)
41. Xiao, J.; Niu, B.; Song, Q.; Zhan, L.; Xu, Z. Novel targetedly extracting lithium: An environmental-friendly controlled chlorinating technology and mechanism of spent lithium ion batteries recovery. *J. Hazard. Mater.* **2021**, *404*, 123947. [\[CrossRef\]](#)
42. Jian, Y.; Zongliang, Z.; Gang, Z.; Liangxing, J.; Fangyang, L.; Ming, J.; Yanqing, L. Process study of chloride roasting and water leaching for the extraction of valuable metals from spent lithium-ion batteries. *Hydrometallurgy* **2021**, *203*, 105638. [\[CrossRef\]](#)
43. Shi, J.; Peng, C.; Chen, M.; Li, Y.; Eric, H.; Klemettinen, L.; Lundström, M.; Taskinen, P.; Jokilaakso, A. Sulfation Roasting Mechanism for Spent Lithium-Ion Battery Metal Oxides Under SO<sub>2</sub>-O<sub>2</sub>-Ar Atmosphere. *JOM* **2019**, *71*, 4473–4482. [\[CrossRef\]](#)
44. Tang, Y.; Qu, X.; Zhang, B.; Zhao, Y.; Xie, H.; Zhao, J.; Ning, Z.; Xing, P.; Yin, H. Recycling of spent lithium nickel cobalt manganese oxides via a low-temperature ammonium sulfation roasting approach. *J. Clean Prod.* **2021**, *279*, 123633. [\[CrossRef\]](#)
45. Yang, C.; Zhang, J.; Cao, Z.; Jing, Q.; Chen, Y.; Wang, C. Sustainable and Facile Process for Lithium Recovery from Spent LiNi<sub>0.8</sub>Co<sub>0.1</sub>Mn<sub>0.1</sub>O<sub>2</sub> Cathode Materials via Selective Sulfation with Ammonium Sulfate. *ACS Sustain. Chem. Eng.* **2020**, *8*, 15732–15739. [\[CrossRef\]](#)
46. Wang, D.; Zhang, X.; Chen, H.; Sun, J. Separation of Li and Co from the active mass of spent Li-ion batteries by selective sulfating roasting with sodium bisulfate and water leaching. *Miner. Eng.* **2018**, *126*, 28–35. [\[CrossRef\]](#)
47. Lin, J.; Li, L.; Fan, E.; Liu, C.; Zhang, X.; Cao, H.; Sun, Z.; Chen, R. Conversion Mechanisms of Selective Extraction of Lithium from Spent Lithium-Ion Batteries by Sulfation Roasting. *ACS Appl. Mater. Interfaces* **2020**, *12*, 18482–18489. [\[CrossRef\]](#)
48. Xu, P.; Liu, C.; Zhang, X.; Zheng, X.; Lv, W.; Rao, F.; Yao, P.; Wang, J.; Sun, Z. Synergic Mechanisms on Carbon and Sulfur during the Selective Recovery of Valuable Metals from Spent Lithium-Ion Batteries. *ACS Sustain. Chem. Eng.* **2021**, *9*, 2271–2279. [\[CrossRef\]](#)
49. Chen, Y.; Shi, P.; Chang, D.; Jie, Y.; Yang, S.; Wu, G.; Chen, H.; Zhu, J.; Hu, F.; Wilson, B.; et al. Selective extraction of valuable metals from spent EV power batteries using sulfation roasting and two stage leaching process. *Sep. Purif. Technol.* **2021**, *258*, 118078. [\[CrossRef\]](#)
50. Pudas, J.; Erkkila, A.; Viljamaa, J. Battery Recycling Method. U.S. Patent 8979006 B2, 17 March 2015.
51. Peng, C.; Liu, F.; Aji, A.; Wilson, B.; Lundström, M. Extraction of Li and Co from industrially produced Li-ion battery waste—Using the reductive power of waste itself. *Waste Manag.* **2019**, *95*, 604–611. [\[CrossRef\]](#)
52. Porvali, A. Complexities of Hydrometallurgical Recycling of Spent NiMH and Li-ion Batteries. Ph.D. Thesis, Aalto University, Espoo, Finland, 2020; pp. 41–42.

**Disclaimer/Publisher's Note:** The statements, opinions and data contained in all publications are solely those of the individual author(s) and contributor(s) and not of MDPI and/or the editor(s). MDPI and/or the editor(s) disclaim responsibility for any injury to people or property resulting from any ideas, methods, instructions or products referred to in the content.